Inorg. Chem. **2007**, *46*, 4128–4137

Redox-Induced Solid–Solid Phase Transformation of TCNQ Microcrystals into Semiconducting $Ni[TCNQ]_2(H_2O)_2$ Nanowire (Flowerlike) Architectures: A Combined Voltammetric, Spectroscopic, and Microscopic Study

Ayman Nafady[†] and Alan M. Bond*

School of Chemistry, Monash University, P.O. Box 23, Victoria 3800, Australia

Received December 25, 2006

The facile solid–solid phase transformation of TCNQ microcrystals into semiconducting and magnetic $Ni[TCNQ]_2(H_2O)_2$ nanowire (flowerlike) architectures is achieved by reduction of TCNQ-modified electrodes in the presence of $Ni^{2+}_{(aq)}$-containing electrolytes. Voltammetric probing revealed that the chemically reversible TCNQ/$Ni[TCNQ]_2(H_2O)_2$ conversion process is essentially independent of electrode material and the identity of nickel counteranion but is significantly dependent on scan rate, $Ni^{2+}_{(aq)}$ electrolyte concentration, and the method of solid TCNQ immobilization (drop casting or mechanical attachment). Data analyzed from cyclic voltammetric and double-potential step chronoamperometric experiments are consistent with formation of the $Ni[TCNQ]_2(H_2O)_2$ complex via a rate-determining nucleation/growth process that involves incorporation of $Ni^{2+}_{(aq)}$ ions into the reduced TCNQ crystal lattice at the triple phase TCNQ|electrode|electrolyte interface. The reoxidation process, which includes the conversion of solid $Ni[TCNQ]_2(H_2O)_2$ back to $TCNQ^0$ crystals, is also controlled by nucleation/growth kinetics. The overall redox process associated with this chemically reversible solid–solid transformation, therefore, is described by the equation: $TCNQ^0_{(S)} + 2e^- + Ni^{2+}_{(aq)} + 2\,H_2O \rightleftharpoons \{Ni[TCNQ]_2(H_2O)_2\}_{(S)}$. SEM monitoring of the changes that accompany the TCNQ/$Ni[TCNQ]_2(H_2O)_2$ transformation revealed that the morphology and crystal size of electrochemically generated $Ni[TCNQ]_2(H_2O)_2$ are substantially different from those of parent TCNQ crystals. Importantly, the morphology of $Ni[TCNQ]_2(H_2O)_2$ can be selectively manipulated to produce either 1-D/2-D nanowires or 3-D flowerlike architectures via careful control over the experimental parameters used to accomplish the solid–solid phase interconversion process.

Introduction

Because of their fascinating structural, electronic, optical, and switching properties, metal−tetracyanoquinodimethane (MTCNQ) charge-transfer complexes have generated substantial interest over the past four decades.[1−13] The outcome of wide ranging research activities, particularly for CuTCNQ, AgTCNQ, and Group I cation (Na^+, K^+, Rb^+, Cs^+)−TCNQ systems,[13−20] is the widespread applications of TCNQ-based

* To whom correspondence should be addressed. Fax: 613-9905-4597. Email: Alan.Bond@sci.monash.edu.au.

[†] Permanent address: Chemistry Department, Sohag University, Sohag, Egypt.

(1) LeBlanc, O. H. Jr. *J. Chem. Phys.* **1965**, *42*, 4307.
(2) Torrance, J. B.; Scott, B. A.; Kaufman, F. B. *Solid State Commun.* **1975**, *17*, 1369.
(3) Potember, R. S.; Poehler, T. O.; Cowan, D. O. *Appl. Phys. Lett.* **1979**, *34*, 405.
(4) Ward, M. D.; Johnson, D. C. *Inorg. Chem.* **1987**, *26*, 4213.
(5) Hertler, W. R.; Mahler, W.; Melby, L. R.; Miller, J. S.; Putscher, R. E.; Webster, O. W. *Mol. Cryst. Liq. Cryst.* **1989**, *171*, 205.
(6) Azcondo, M. T.; Ballester, L.; Golhen, S.; Gutierrez, A.; Ouahab, L.; Yartsev, S.; Delhaes, P. *J. Mater. Chem.* **1999**, *9*, 1237.
(7) Miyasaka, H.; Campos-Fernandez, C. S.; Clerac, R.; Dunbar, K. R. *Angew. Chem., Int. Ed.* **2000**, *39*, 3831.
(8) Pokhodnya, K. I.; Petersen, N.; Miller, J. S. *Inorg. Chem.* **2002**, *41*, 1996.
(9) Kuroda, N.; Sugimoto, T.; Hagiwara, M.; Hasanudin; Ueda, K.; Tada, T.; Uozaki, H.; Toyota, N.; Mogi, I.; Watanabe, K.; Motokawa, M. *Synth. Met.* **2003**, *133−134*, 535.
(10) Kaur, P.; Sarangal, A.; Hundal, G.; Rao, T. V. C. *J. Coord. Chem.* **2005**, *58*, 495.
(11) Fan, Z. Y.; Mo, X. L.; Lou, C. F.; Yao, Y.; Wang, D. W.; Chen, G. R.; Lu, J. G. *IEEE Trans. Nanotechnol.* **2005**, *4*, 238.
(12) Taliaferro, M. L.; Palacio, F.; Miller, J. S. *J. Mater. Chem.* **2006**, *16*, 2677.
(13) Miyasaka, H.; Izawa, T.; Takahashi, N.; Yamashita, M.; Dunbar, K. R. *J. Am. Chem. Soc.* **2006**, *128*, 11358.
(14) Potember, R. S.; Poehler, T. O.; Benson, R. C. *Appl. Phys. Lett.* **1982**, *41*, 548.

10.1021/ic062470l CCC: $37.00
Published on Web 04/21/2007

molecular materials in information storage media,[21−24] organic field-effect transistors,[25−27] sensors,[28−31] and electrochromic and magnetic devices.[32−34] In recent years, much effort has been devoted to the synthesis and fabrication of well-controlled MTCNQ micro/nanostructures,[35−38] because their sizes and morphologies are generally believed to be key elements in the tuning of their intrinsic chemical and physical properties.[39−41] Thus, various synthetic methods including direct reaction of $TCNQ^-$ with metal salts, vapor deposition of TCNQ on metal surfaces, and spontaneous electrolysis and electrospinning, along with other photochemical and electrochemical techniques, have been used to accomplish this goal.[35−38,42−48]

In contrast, the conceptually related semiconducting binary $M[TCNQ]_2$-based materials (M = first-row transition metal) have been far less studied.[49−51] However, the recent discovery of novel magnetic properties has motivated significant interest because of their relevance to the field of molecule-based solid-state chemistry.[52−55] Central to these studies, the research groups of Dunbar and Miller have developed different synthetic methodolgies for the chemical synthesis and characterization of different forms of these materials. These include the hydrated $M[TCNQ](H_2O)_2$ phase, which is of particular interest to this paper, the alcoholic $M[TCNQ](MeOH)_2$ analogue, and solvent-free $M[TCNQ]_2$ (M = Mn, Fe, Co, Ni) "glassy magnets".[56−58] A persistent synthetic obstacle that is evident from these reports is the low solubility of these polymeric materials in most solvents, which makes their recrystallization and purification into crystalline forms extremely difficult. This and related problems[52] have hampered the investigation and potential application of the $M[TCNQ]_2$-based materials in magnetic and electronic devices.

Previous work from our laboratory on the 1:1 MTCNQ family (M = Cu^+, Group I cations)[30,42,45,59−61] and, more recently, on the binary $Co[TCNQ]_2(H_2O)_2$ analogue[62] has shown that generic electrochemical techniques may be available for facile and controllable synthesis of many classes of $M^{n+}[TCNQ]_n$ charge-transfer complexes by redox-induced solid−solid phase conversion of suitable TCNQ-modified electrodes immersed in aqueous solution of $M^{n+}_{(aq)}$ electrolytes. Furthermore, this simple approach has significantly enhanced the understanding of the morphological and crystal size changes that accompany the solid−solid transformation processes along with establishing some aspects of the mechanism that controls the relevant redox chemistry.

In this paper, we used procedures established in earlier studies to electrochemically induce the solid−solid phase transformation of microcrystalline TCNQ-modified electrodes placed in contact with aqueous $Ni^{2+}_{(aq)}$ electrolytes into semiconducting and magnetic $Ni[TCNQ]_2(H_2O)_2$ nanowire architectures. In addition to the spectroscopic (IR, Raman)

(15) Hoagland, J. J.; Wang, X. D.; Hipps, K. W. *Chem. Mater.* **1993**, *5*, 54.
(16) Gu, N.; Yang, X.-M.; Sheng, H.-Y.; Lu, W.; Wei, Y. *Synth. Met.* **1995**, *71*, 2221.
(17) Sun, S.; Xu, X.; Wu, P.; Zhu, D. *J. Mater. Sci. Lett.* **1998**, *17*, 719.
(18) Mo, X.-L.; Chen, G.-R.; Cai, Q.-J.; Fan, Z.-Y.; Xu, H.-H.; Yao, Y.; Yang, J.; Gu, H.-H.; Hua, Z.-Y. *Thin Solid Films* **2003**, *436*, 259.
(19) Liu, Y.; Ji, Z.; Tang, Q.; Jiang, L.; Li, H.; He, M.; Hu, W.; Zhang, D.; Jiang, L.; Wang, X.; Wang, C.; Liu, Y.; Zhu, D. *Adv. Mater.* **2005**, *17*, 2953.
(20) Muller, R.; Genoe, J.; Heremans, P. *Appl. Phys. Lett.* **2006**, *88*, 242105.
(21) Cho, O. K.; Park, K. Y. *Mol. Cryst. Liq. Cryst.* **1995**, *267*, 393.
(22) Yamaguchi, S.; Potember, R. S. *Synth. Met.* **1996**, *78*, 117.
(23) Fan, Z. Y.; Mo, X. L.; Chen, G. R.; Lu, J. G. *Rev. Adv. Mater. Sci.* **2003**, *5*, 72.
(24) Peng, H.; Chen, Z.; Tong, L.; Yu, X.; Ran, C.; Liu, Z. *J. Phys. Chem. B* **2005**, *109*, 3526.
(25) Brown, A. R.; de Leeuw, D. M.; Lous, E. J.; Havinga, E. E. *Synth. Met.* **1994**, *66*, 257.
(26) Menard, E.; Podzorov, V.; Hur, S. H.; Gaur, A.; Gershenson, M. E.; Rogers, J. A. *Adv. Mater.* **2004**, *16*, 2097.
(27) Di, C.-a.; Yu, G.; Liu, Y.; Xu, X.; Wei, D.; Song, Y.; Sun, Y.; Wang, Y.; Zhu, D.; Liu, J.; Liu, X.; Wu, D. *J. Am. Chem. Soc.* **2006**, *128*, 16418.
(28) Wakida, S.-i.; Kohigashi, Y.; Miyamura, H.; Higashi, K.; Ujihira, Y. *Anal. Sci.* **1996**, *12*, 989.
(29) Palmisano, F.; Zambonin, P. G.; Centonze, D.; Quinto, M. *Anal. Chem.* **2002**, *74*, 5913.
(30) Wooster, T. J.; Bond, A. M. *Analyst* **2003**, *128*, 1386.
(31) Cano, M.; Palenzuela, B.; Rodriguez-Amaro, R. *Electroanalysis* **2006**, *18*, 1068.
(32) Yasuda, A.; Seto, J. *J. Electroanal. Chem.* **1988**, *247*, 193.
(33) Perepichka, D. F.; Bryce, M. R.; Pearson, C.; Petty, M. C.; McInnes, E. J. L.; Zhao, J. P. *Angew. Chem., Int. Ed.* **2003**, *42*, 4636.
(34) Valade, L.; de Caro, D.; Malfant, I. *NATO Sci. Ser., II: Math, Phys. Chem.* **2004**, *139*, 241.
(35) Muller, R.; De Jonge, S.; Myny, K.; Wouters, D. J.; Genoe, J.; Heremans, P. *Solid-State Electron.* **2006**, *50*, 601.
(36) Shang, T.; Yang, F.; Zheng, W.; Wang, C. *Small* **2006**, *2*, 1007.
(37) Liu, Y.; Li, H.; Tu, D.; Ji, Z.; Wang, C.; Tang, Q.; Liu, M.; Hu, W.; Liu, Y.; Zhu, D. *J. Am. Chem. Soc.* **2006**, *128*, 12917.
(38) O'Mullane, A. P.; Fay, N; Nafady, A.; Bond, A. M. *J. Am. Chem. Soc.* **2007**, *129*, 2066.
(39) Alivisatos, A. P. *Science* **1996**, *271*, 933.
(40) Burda, C.; Chen, X.; Narayanan, R.; El-Sayed, M. A. *Chem. Rev.* **2005**, *105*, 1025.
(41) Neufeld, A. K.; O'Mullane, A. P.; Bond, A. M. *J. Am. Chem. Soc.* **2005**, *127*, 13846.
(42) Bond, A. M.; Fletcher, S.; Symons, P. G. *Analyst* **1998**, *123*, 1891.
(43) Heintz, R. A.; Zhao, H.; Ouyang, X.; Grandinetti, G.; Cowen, J.; Dunbar, K. R. *Inorg. Chem.* **1999**, *38*, 144.
(44) O'Kane, S. A.; Clerac, R.; Zhao, H.; Ouyang, X.; Galan-Mascaros, J. R.; Heintz, R.; Dunbar, K. R. *J. Solid State Chem.* **2000**, *152*, 159.
(45) Neufeld, A. K.; Madsen, I.; Bond, A. M.; Hogan, C. F. *Chem. Mater.* **2003**, *15*, 3573.
(46) Harris, A. R.; Neufeld, A. K.; O'Mullane, A. P.; Bond, A. M.; Morrison, R. J. S. *J. Electrochem. Soc.* **2005**, *152*, C577.
(47) Liu, Y.; Ji, Z.; Tang, Q.; Jiang, L.; Li, H.; He, M.; Hu, W.; Zhang, D.; Jiang, L.; Wang, X.; Wang, C.; Liu, Y.; Zhu, D. *Adv. Mater.* **2005**, *17*, 2953.
(48) Cao, G.; Ye, C.; Fang, F.; Xing, X.; Xu, H.; Sun, D.; Chen, G. *Micron* **2005**, *36*, 267.
(49) Melby, L. R.; Harder, R. J.; Hertler, W. R.; Mahler, W.; Benson, R. E.; Mochel, W. E. *J. Am. Chem. Soc.* **1962**, *84*, 3374.
(50) Siedle, A. R.; Candela, G. A.; Finnegan, T. F. *Inorg. Chim. Acta* **1979**, *35*, 125.
(51) Kathirgamanathan, P.; Rosseinsky, D. R. *J. Chem. Soc., Chem. Commun.* **1980**, 839.
(52) Zhao, H.; Heintz, R. A.; Dunbar, K. R.; Rogers, R. D. *J. Am. Chem. Soc.* **1996**, *118*, 12844.
(53) Zhao, H.; Heintz, R. A.; Ouyang, X.; Grandinetti, G.; Cowen, J.; Dunbar, K. R. *NATO ASI Ser., Ser. C* **1999**, *518*, 353.
(54) Long, G.; Willett, R. D. *Inorg. Chim. Acta* **2001**, *313*, 1.
(55) Vickers, E. B.; Selby, T. D.; Thorum, M. S.; Taliaferro, M. L.; Miller, J. S. *Inorg. Chem.* **2004**, *43*, 6414.
(56) Zhao, H.; Heintz, R. A.; Ouyang, X.; Dunbar, K. R.; Campana, C. F.; Rogers, R. D. *Chem. Mater.* **1999**, *11*, 736.
(57) Clerac, R.; O'Kane, S.; Cowen, J.; Ouyang, X.; Heintz, R.; Zhao, H.; Bazile, M. J., Jr.; Dunbar, K. R. *Chem. Mater.* **2003**, *15*, 1840.
(58) Vickers, E. B.; Giles, I. D.; Miller, J. S. *Chem. Mater.* **2005**, *17*, 1667.
(59) Bond, A. M.; Fletcher, S.; Marken, F.; Shaw, S. J.; Symons, P. G. *J. Chem. Soc., Faraday Trans.* **1996**, *92*, 3925.
(60) Suarez, M. F.; Bond, A. M.; Compton, R. G. *J. Solid State Electrochem.* **1999**, *4*, 24.
(61) O'Mullane, A. P.; Neufeld, A. K.; Bond, A. M. *Anal. Chem.* **2005**, *77*, 5447.
(62) Nafady, A.; O'Mullane, A. P.; Bond, A. M.; Neufeld, A. K. *Chem. Mater.* **2006**, *18*, 4375.

and microscopic (SEM) characterization of the structure and morphology of this electrosynthesized material, we also offer new insights into mechanistic aspects of its formation. Significantly, different morphologies of the electrochemically produced $Ni[TCNQ]_2(H_2O)_2$, including one-dimensional (1-D) bundles, 2-D/3-D nanowires/nanorods, and 3-D flower-like architectures, could be achieved by controlling the method of electrode modification and voltammetric protocol employed. Thus, the present study opens up new opportunities to understand the intrinsic chemical and physical properties of the molecule-based $M[TCNQ]_2$ family and hence foster their application in nanoelectronic and other devices.

Experimental Section

Materials and Synthesis of $Ni[TCNQ]_2(H_2O)_2$. Analytical grade hydrated $Ni(ClO_4)_2 \cdot 6H_2O$ and $Ni(NO_3)_2 \cdot 6H_2O$, TCNQ (98%) (Aldrich), and acetonitrile (HPLC grade, Omnisolv) were used as received from the suppliers. $Ni[TCNQ]_2(H_2O)_2$ was chemically prepared and characterized according to procedures described by Dunbar and co-workers.[56]

Electrochemistry. Aqueous electrolytes used in electrochemical studies were prepared using water purified in a Millipore system (resistivity 18.2 MΩ cm). Electrochemical measurements were undertaken at 293 ± 2 K with an Autolab PGSTAT100 (ECO-Chemie) workstation and a standard three-electrode cell configuration. For voltammetric and potential-step experiments, glassy carbon (GC) disk (3 mm diameter, Bioanalytical Systems), platinum (Pt), and gold (Au) (1.6 mm diameter, Bioanalytical Systems), as well as indium tin oxide (ITO)-coated glass (0.06−0.1 cm^2 area) with a 10 Ω/sq sheet resistance (as quoted by the manufacturer Prazisions Glas and Optik GmbH), were used as the working electrodes. The procedures employed for polishing these electrodes are described elsewhere.[62] The reference electrode was an aqueous Ag/AgCl (3 M KCl, Bioanalytical Systems), and the counter electrode was made from platinum mesh. A stream of N_2 gas was used to sparge the aqueous solutions in which chemically modified TCNQ electrodes were placed, and a flow of this gas was maintained above the solution during the course of electrochemical experiments.

Electrode Modification. Immobilization of solid TCNQ onto the surface of GC, ITO, or metal electrodes was undertaken by either the drop casting or mechanical attachment methods.[62] In the former approach, the working electrode was dipped into a 10 mM acetonitrile solution of TCNQ. The electrode was then removed from the solution and hung face down. Upon evaporation of the acetonitrile, an array of TCNQ crystals was formed. In the case of the ITO electrode, the surface was modified by application of 10−20 μL ($1-2 \times 10^{-7}$ mol) droplets of 10 mM TCNQ acetonitrile solution over the surface. These procedures also gave rise to an array of regularly spaced large TCNQ microcrystals with a rhombic shape (vide infra). In the second approach of immobilization, a small amount of TCNQ microcrystals was transferred to a piece of weighing paper over which the electrode was rubbed, thus causing the TCNQ nanoparticles to adhere to the electrode surface. The mechanical attachment method leads to the immobilization of a greater quantity of smaller TCNQ particles on the electrode surface (vide infra).

Physical Measurements. Infrared spectroscopy (IR), scanning electron microscopy (SEM), and energy-dispersive X-ray (EDAX) experiments were carried out as previously described.[62] Raman spectra were obtained with a Renishaw RM 2000 Raman spectrograph and microscope using an 18 mW, 780 nm excitation source.

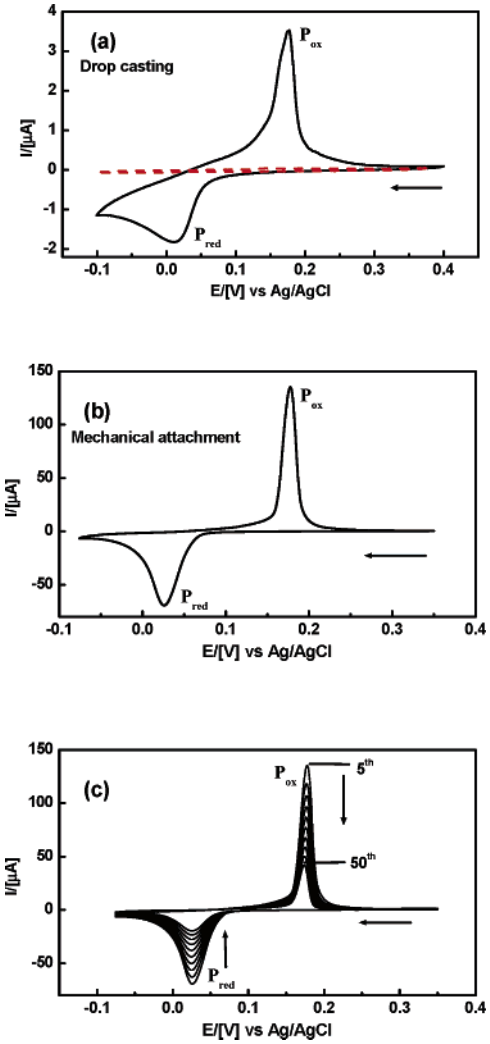

Figure 1. (a) Cyclic voltammograms obtained with a scan rate of 20 mV s^{-1} for the fifth cycle of the potential over the range of 0.35 to −0.075 V at a bare surface (----) and at a drop cast TCNQ-modified GC disk electrode in contact with 0.1 M $Ni(NO_3)_{2(aq)}$ electrolyte, (b) with a GC electrode modified with TCNQ via the mechanical attachment method, and (c) for cycles 5−50 of the potential with every fifth cycle being shown.

Results and Discussion

I. Voltammetric Probing of the Redox-Induced TCNQ/$Ni[TCNQ]_2(H_2O)_2$ Solid−Solid-Phase Transformation. I.A. Reduction of Solid TCNQ in the Presence of $Ni^{2+}_{(aq)}$ Electrolyte. Cyclic voltammograms obtained with TCNQ-modified GC electrodes (via either drop casting or mechanical attachment) immersed in aqueous solution containing 0.1 M $Ni(NO_3)_2$, where the potential is initially scanned in the negative direction from 0.35 to −0.075 V vs Ag/AgCl at a rate of 20 mV s^{-1}, are shown in Figure 1. Despite the inherent complexity associated with the initial cycles of potential, after several (3−5) potential cycles, well-defined reduction peaks (P_{red}) at ∼0.011 V and sharper and more intense oxidation peaks (P_{ox}) at 0.175 V (Figure 1a) are detected when the drop casting method is used to immobilize

TCNQ. GC-electrodes modified with TCNQ via the mechanical attachment method gave rise to simpler and more reproducible cyclic voltammograms having sharp, well-separated, symmetrical reduction and oxidation components even in the initial potential cycles (Figure 1b). Under these conditions, P_{red} appears at $E_p^{red} = 0.025$ V, and P_{ox} has a value for E_p^{ox} of 0.178 V. A large peak-to-peak separation ($\Delta E_p = E_p^{ox} - E_p^{red} = 153$ mV) or "inert zone" is consistent with expectation for an assumed electrochemically irreversible TCNQ/Ni[TCNQ]$_2$ solid−solid phase conversion governed by nucleation/growth kinetics.[59,62−64] However, ΔE_p for nickel is significantly smaller than that obtained for the TCNQ/Co[TCNQ]$_2$(H$_2$O)$_2$ (226 mV)[62] and other TCNQ/MTCNQ (M = Cu$^+$, K$^+$, Na$^+$, and Cs$^+$)[42,45] solid−solid conversions, thereby indicating that the identity of the cation plays a crucial role in the kinetic of the redox-induced transformation of solid TCNQ into the corresponding M^{n+}-[TCNQ]$_n$ materials.

Analysis of the voltammetric data extracted from Figure 1b revealed that despite the peak width at half-height for the reduction process ($W_{1/2}^{red} = 39$ mV) being drastically larger than that of the oxidation process ($W_{1/2}^{ox} = 18$ mV), the peak areas associated with this redox cycle are quantitatively similar (viz., area (A) of $P_{red} = 1.70 \times 10^{-4}$ C and that of $P_{ox} = 1.68 \times 10^{-4}$ C). This behavior implies that a high level of chemical reversibility of the TCNQ/Ni[TCNQ]$_2$ conversion process is associated with initial cycles. Despite the slight attenuation in peak heights with each scan, chemical reversibility is almost maintained upon continuous cycling of the potential over the range from 0.35 to −0.075 V. For example, for the fifth cycle in Figure 1c, $Q_{red} = -1.87 \pm 0.23 \times 10^{-4}$ C, whereas $Q_{ox} = 1.79 \pm 0.22 \times 10^{-4}$ C. Upon even more extensive cycling of the potential (50 cycles), the peak currents continue to be reduced in height, and the charges associated with processes P_{red} and P_{ox} decrease to -6.11×10^{-5} and 5.50×10^{-5} C, respectively, but otherwise the principal features of the cyclic voltammograms are retained, as illustrated in Figure 1c. This decrease in peak current heights during the course of cycling the potential mimics the results reported for the electrochemical conversion of TCNQ to the Co[TCNQ]$_2$-(H$_2$O)$_2$ analogue.[62] Thus, this behavior is most likely caused by a small level of dissolution of TCNQ[42] or the electrochemically generated Ni[TCNQ]$_2$-based material in aqueous media.[57]

The detection of only one oxidation process, even after prolonged potential-cycling experiments, indicates that only one phase of Ni[TCNQ]$_2$-based material is formed. This is most likely to be Ni[TCNQ]$_2$(H$_2$O)$_2$ which is the stable form of Ni[TCNQ]$_2$ synthesized from aqueous media.[56] On the basis of this assumption, the reactions involved in the redox-induced chemically reversible TCNQ/Ni[TCNQ]$_2$(H$_2$O)$_2$ interconversion process are likely to be described by eqs 1 and 2. The inclusion of Ni$^{2+}_{(aq)}$ ions from bulk solution (eq 1) and its exclusion (eq 2) from the TCNQ/TCNQ$^-$ crystal lattice is expected to occur more easily in the smaller mechanically attached particles than in the considerably larger TCNQ microcrystals produced by the drop casting method. However, in the latter case, crystal fragmentation into smaller particles takes place in the initial redox sequences of the TCNQ/Ni[TCNQ]$_2$(H$_2$O)$_2$ scans, as evident by SEM images (vide infra). Thus, the differences in immobilized TCNQ crystal sizes and morphologies probably account for the dependence of the voltammetry on the method of electrode modification.

$$2\mathrm{TCNQ}_{(s,GC)} + \mathrm{Ni}^{2+}_{(aq)} + 2e^- + 2\mathrm{H_2O} \xrightarrow{P_{red}} \{\mathrm{Ni[TCNQ]_2(H_2O)_2}\}_{(s,GC)} \quad (1)$$

$$\{\mathrm{Ni[TCNQ]_2(H_2O)_2}\}_{(s,GC)} \xrightarrow{P_{ox}} \mathrm{Ni}^{2+}_{(aq)} + 2\mathrm{TCNQ}_{(s,GC)} + 2\mathrm{H_2O} + 2e^- \quad (2)$$

Analogously to the TCNQ/Co[TCNQ]$_2$(H$_2$O)$_2$ system,[62] voltammetric responses for the nickel case with different electrode materials including GC, metallic (Pt, Au), and semiconducting (ITO) and with different Ni(II) counteranions (e.g., ClO_4^-, NO_3^-, Cl^-, and SO_4^{2-}) were virtually identical. Thus, both the electrode material and the identity of the Ni^{2+} counteranion do not appear to play a significant role in the redox-induced TCNQ/Ni[TCNQ]$_2$(H$_2$O)$_2$ transformation process. However, a marked dependence on the Ni$^{2+}_{(aq)}$ concentration and scan rate was found.

I.B. Influence of Ni$^{2+}_{(aq)}$ Concentration. Figure 2 shows the dependence of cyclic voltammograms obtained at a scan rate of 10 mV s^{-1} for the TCNQ/Ni[TCNQ]$_2$(H$_2$O)$_2$ interconversion process on the concentration of Ni$^{2+}_{(aq)}$ (0.001−1.0 M). At low Ni$^{2+}_{(aq)}$ concentration (0.001 M), both severe broadening of the oxidation and reduction peaks and a marked increase in the peak separation are observed. This is attributed to the high level of uncompensated resistance (R_u) and hence the iR_u drop encountered with this low electrolyte concentration. For this reason, quantitative analysis of the voltammetric data is limited to the 0.01−1.0 M Ni$^{2+}_{(aq)}$ concentration range.

Thermodynamically and kinetically relevant parameters[30] may be derived from the reversible (E_R) or midpoint (E_m) potentials (eqs 3 and 4) and the peak separation (ΔE_p) (eq 5), respectively. If the over-potentials associated with the reduction (E_p^{red}) and oxidation (E_p^{ox}) processes are equal, then E_m will be equal to E_R. A plot of E_m versus log [Ni^{2+}] (Figure S1) exhibits a slope of $S = 34 \pm 4$ mV. This is close to the value of about 30 mV,[30] with $n = 2$, predicted from the 2.303RT/nF parameter of the Nernst equation. This result implies that ohmic drop influences are small and the activity of the reduced and oxidized solid phases are both close to unity. The dependence of ΔE_p on nickel ion

$$E_R = \text{constant} - 2.303RT/nF \log [\mathrm{Ni}^{2+}] \quad (3)$$

$$E_m = (E_p^{red} + E_p^{ox})/2 = \text{constant} - S \log [\mathrm{Ni}^{2+}] \quad (4)$$

$$\Delta E_p = E_p^{red} - E_p^{ox} \quad (5)$$

(63) Fletcher, S.; Halliday, C. S.; Gates, D.; Westcott, M.; Lwin, T.; Nelson, G. *J. Electroanal. Chem.* **1983**, *159*, 267.
(64) Suarez, M. F.; Marken, F.; Compton, R. G.; Bond, A. M.; Miao, W.; Raston, C. L. *J. Phys. Chem. B* **1999**, *103*, 5637.

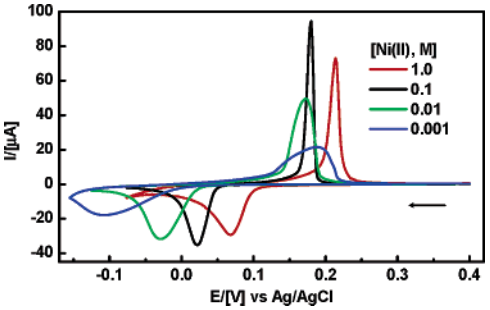

Figure 2. Cyclic voltammograms obtained at scan rate of 10 mV s^{-1} (third cycle of potential shown) with a TCNQ-modified GC electrode (mechanical attachment method) immersed in aqueous $Ni(NO_3)_{2(aq)}$ electrolyte at designated concentrations.

Table 1. Voltammetric Parameters[a] Obtained at a Scan Rate of 10 mV s^{-1} for a TCNQ-modified GC Electrode (Mechanical Attachment Method) Immersed in Different Concentrations of $Ni(NO_3)_{2\ (aq)}$ Solution[b]

$[Ni^{2+}_{(aq)}]$ (M)	E_p^{red} (V)	$W_{1/2}^{red}$ (mV)	E_p^{ox} (V)	$W_{1/2}^{ox}$ (mV)	E_m (V)	ΔE_p (V)
1.0	0.068	47	0.213	13	0.141	0.145
0.1	0.021	31	0.179	10	0.100	0.158
0.01	−0.029	52	0.172	32	0.072	0.201
0.001	−0.096	103	0.187	70	0.045	0.283

[a] E_m represents the midpoint potential measured as $(E_p^{red} + E_p^{ox})/2$ in volts versus Ag/AgCl (3 M KCl); ΔE_p is the peak potential separation calculated as $(E_p^{ox} - E_p^{red})$. E_p^{red} and E_p^{ox} are reduction and oxidation peak potentials respectively; $W_{1/2}^{red}$ and $W_{1/2}^{ox}$ are the peak widths at half-height for the reduction and oxidation components respectively. [b]Voltammetric data were collected after 5 cycles of the potential.

concentration (Table 1, Figure S1) is probably influenced by the ohmic potential drop, which will be very substantial, particularly when only 0.001 M of $Ni(NO_3)_2$ is present to act as an electrolyte. In contrast, ohmic drop effects should be minimal for nickel concentration of ≥0.1 M. Fortunately, the E_m values, which are derived as an average of $(E_p^{ox} + E_p^{red})/2$, are almost corrected for iR_u drop. However, increased $W_{1/2}$ values resulting from the change in the $Ni^{2+}_{(aq)}$ concentration from 0.1 to 1.0 M are not explicable via the iR_u drop; therefore, other mechanistic nuances that contribute to the reduction and oxidation components must be present.

I.C. Voltammetric and Chronoamperometric Detection of Nucleation/Growth Kinetics. (a) Scan Rate and Switching Potential Effects. Figure 3a contains representative cyclic voltammograms obtained as a function of scan rate (ν) for the conversion of TCNQ into the $Ni[TCNQ]_2(H_2O)_2$ complex when the modified GC electrode (mechanical attachment method) is placed in contact with 0.1 M $Ni^{2+}_{(aq)}$ ions. The iR_u drop effects under these conditions should be small. Inspection of the voltammetric data extracted from these cyclic voltammograms (Table 2) demonstrates that both E_p^{red} and E_p^{ox} are markedly influenced by increasing the scan rate from 5.0 to 50 mV s^{-1}. Thus, E_p^{red} shifts to more negative by 37 mV while E_p^{ox} becomes more positive (29 mV shift) over this scan rate range. $W_{1/2}$ and ΔE_p also are significantly increased, but E_m remains almost constant, as expected for a thermodynamically significant parameter. The dependence of the aforementioned voltammetric parameters on scan rate is indicative of nucleation/growth kinetics.[42,62]

In principle, the nature of the nucleation/growth process may be established by analysis of the scan rate variation of

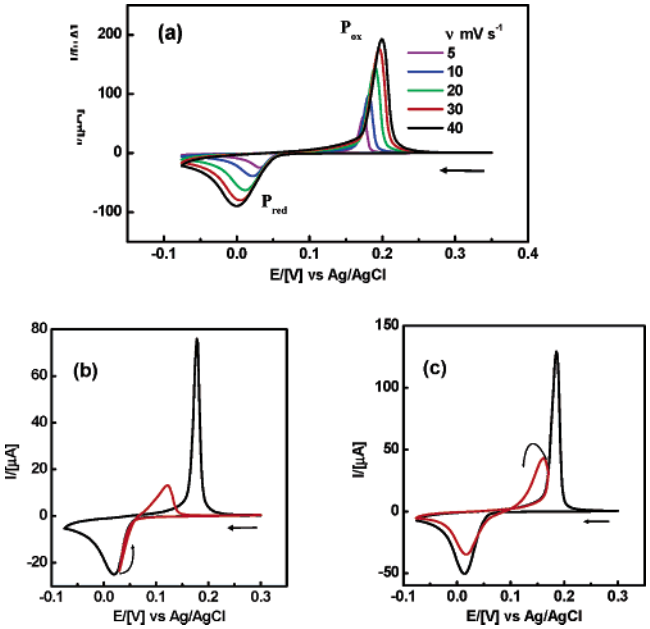

Figure 3. (a) Cyclic voltammograms obtained with a TCNQ-modified GC electrode (mechanical attachment) in contact with 0.1 M $Ni(NO_3)_{2(aq)}$ solution at designated scan rates. (b) Cyclic voltammograms obtained under same conditions as in panel (a) with a scan rate of 0.020 V s^{-1}. Fourth cycle shown followed by the fifth cycle when the potential is switched at the foot of the reduction wave, which induces a hystereses loop into the voltammogram, as indicated by the arrows. (c) Cyclic voltammograms obtained under same conditions as in b, but on the fifth cycle, the potential is switched at the foot of the oxidation wave, as indicated by the arrows.

Table 2. Voltammetric Parameters Obtained as a Function of Scan Rate for a TCNQ-Modified GC Electrode (Mechanical Attachment Method) Placed in Contact with a 0.1 M $Ni(NO_3)_{2(aq)}$ Solution[a]

scan rate (mVs^{-1})	E_p^{red} (V)	$W_{1/2}^{red}$ (mV)	Q_{red} (μC)	E_p^{ox} (V)	$W_{1/2}^{ox}$ (V)	Q_{ox} (μC)	E_m (mV)	ΔE_p (mV)
5	0.032	29	275	0.174	11	230	103	142
10	0.021	39	244	0.181	15	210	102	160
20	0.011	48	216	0.190	19	195	101	179
30	0.005	56	197	0.196	21	182	100	191
40	−0.001	60	177	0.200	23	168	100	201
50	−0.005	66	156	0.203	26	147	99	208

[a] Voltammetric data collected after 3 redox cycles over the potential range from 0.35 to −0.075 V. The symbols in headings are defined in Table 1.

the voltammetric peaks for both the reduction (P_{red}) and oxidation (P_{ox}) components in terms of predictions based on theoretical models developed for 2-D nucleation/growth mechanisms and recently applied to the KTCNQ system.[65] According to these models, the generated log−log plots of i_p, $W_{1/2}$, and ΔE_p as a function of scan rate should be linear and have slopes of x, $1 - x$, and $1 - x$, respectively, where x is 0.6 or slightly higher.[65] Indeed, with the mechanical attachment method of electrode modification, plot of log i_p and log $W_{1/2}$ for processes P_{red} and P_{ox}, and log ΔE_p versus log ν established linear dependencies with the estimated slopes given in Table 3. The slopes of the log−log plots of i_p and $W_{1/2}$ are in a good agreement with the predictions of 2-D phase transitions and similar to the values reported for KTCNQ.[65] The slope of the log ΔE_p plot (0.17) is smaller than the expected theoretical value (0.4) but closer to the

(65) Gomez, L.; Rodriguez-Amaro, R. *Langmuir* **2006**, *22*, 7431 and references therein.

Table 3. Extracted Voltammetric Data of log−log Plots of i_p, $W_{1/2}$, and ΔE_p versus ν over the Entire Range of the Scan Rate (5−50 mV s^{-1})

process/slope	log i_p vs log ν	log $W_{1/2}$ vs log ν	log ΔE_p vs log ν
P_{red}	0.59 ± 0.03	0.35 ± 0.01	0.17 ± 0.01
P_{ox}	0.52 ± 0.03	0.36 ± 0.02	

experimental value (0.1) obtained for the KTCNQ system.[65] Thus, processes P_{red} and P_{ox} are suggested to contain "layer-by-layer" 2-D nucleation/growth, with the ingress of $Ni^{2+}_{(aq)}$ ions from bulk solution onto the growing $TCNQ^-$ nuclei being the rate-determining step. This conclusion will also be partly supported by SEM images (vide infra) obtained for ITO electrodes modified with TCNQ via the mechanical attachment method. However, the anomalous ΔE_p dependence relative to theoretical predictions and features such as voltammograms being a function of the state of the TCNQ initially present suggest that the process must be more complex than 2-D growth and might include 3-D growth as well.

Further evidence for nucleation/growth kinetics is obtained from cyclic voltammetric scans via observation of current loops and maxima when the potential direction is reversed at the foot of either the reduction (Figure 3b) or oxidation (Figure 3c) components of the redox processes. These phenomena are diagnostic of nucleation/growth kinetics.[42]

(b) Chronoamperometry. Detection of nucleation/growth kinetics also is found by even causal inspection of double-potential step chronoamperometric experiments.[59,62−64] Results for a TCNQ-modified GC electrode (mechanical attachment method) subjected to at least 5 cycles over the potential range (0.35 to −0.075 V) at a scan rate of 20 mV s^{-1} are presented in Figure 4. Figure 4a provides current−time ($i-t$) curve obtained by initially stepping the potential from an initial value (E_i = 300 mV), where no faradaic process occurs, to a more negative value (E_{red} = 10 mV) to induce reduction of TCNQ into $TCNQ^-$ and hence formation of Ni[TCNQ]$_2$(H$_2$O)$_2$ (process P_{red}). After 30 s, the potential is stepped back to E_{ox} = 190 mV to induce oxidation process P_{ox}. Maxima characteristic for the presence of a rate-determining nucleation/growth process[42] are detected for both P_{red} and P_{ox}, under these and related conditions (Figure 4b and c), but are more pronounced for process P_{ox} than P_{red}.

On the basis of cyclic voltammetric and chronoamperometric data, it is concluded that the redox-induced transformation of TCNQ microcrystals immobilized on the surface of a GC electrode in contact with an aqueous solution of Ni^{2+} ions represents a chemically reversible solid−solid phase transformation that is governed by nucleation/growth kinetics as previously reported for other $M^{n+}[TCNQ]_n$ systems (M = Co^{2+}, Cu^+, or Group I cations; n = 1 or 2).[42,45,62]

II. Spectroscopic Confirmation of Ni[TCNQ]$_2$(H$_2$O)$_2$ Formation. II.A. IR Spectroscopy. The IR spectrum of the solid formed as a result of 10.5 potential cycles over the range from 0.35 to −0.05 V of a TCNQ-modified GC or ITO electrode in the presence of 0.1 M $Ni^{2+}_{(aq)}$ electrolyte is displayed in Figure S2. Three resolved IR bands in the ν(C≡N) region at 2225, 2206, and 2179 cm^{-1} are in

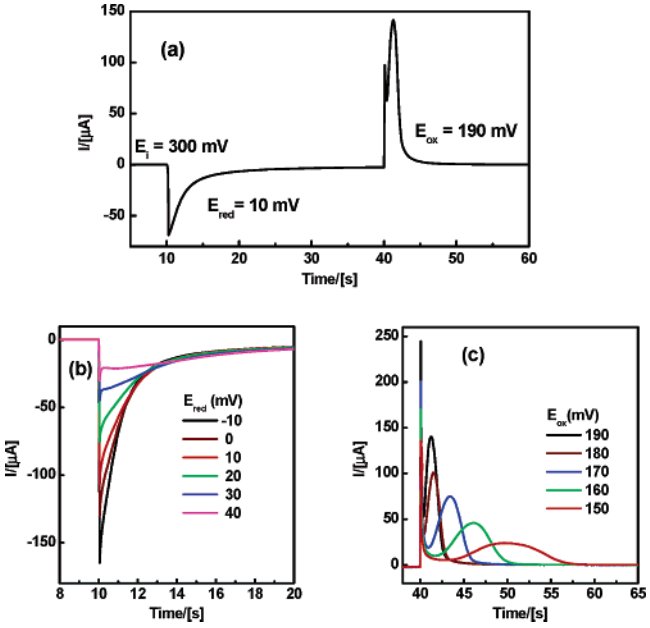

Figure 4. Double-potential step chronoamperograms obtained when a GC electrode modified with microcrystals of TCNQ (mechanical attachment) is in contact with 0.1 M Ni(NO$_3$)$_{2(aq)}$: (a) $i-t$ transient obtained when the potential initially is stepped from E_i = 300 to E_{red} = 10 mV for 30 s to induce reduction and then back to E_{ox} = 190 mV to induce oxidation, (b) $i-t$ curves obtained under same electrode conditions as in panel a when the potential is stepped from E_i = 300 mV to the designated (E_{red}) potentials to induce reduction and then back to E_{ox} = 190 mV in each case to induce oxidation, and (c) $i-t$ curves obtained when the potential is stepped from E_i = 300 mV to E_{red} = 10 mV to induce reduction and then back to designated (E_{ox}) potentials to induce oxidation. These data were collected after 5 cycles of the potential over the range from 300 to 50 mV.

Table 4. Infrared Absorption Frequencies Obtained for Ni[TCNQ]$_2$(H$_2$O)$_2$, Prepared Chemically and Electrochemically

method of preparation	δ(C−H) (cm^{-1})	ν(C=C) (cm^{-1})	ν(C≡N) (cm^{-1})
chemical synthesis[a]	823 m	1505 s	2226 s, 2207 s, 2177 m
electrolysis[b]	824 m	1504 s	2224 s, 2204 s, 2179 s
cyclic voltammetry[c]	825 m	1506 s	2225 s, 2206 s, 2179 s

[a] Reaction of aqueous solution of Ni(NO$_3$)$_2$ with LiTCNQ.[56] [b] Bulk electrolysis at −0.05 V for 10 min of a TCNQ-modified ITO electrode in the presence of 0.1 M Ni(NO$_3$)$_2$·6H$_2$O. [c] After 10.5 potential cycles over the range from 0.3 to −0.05 V at a scan rate of 20 mV s^{-1} with either a TCNQ-modified GC or ITO electrode.

agreement with the presence of $TCNQ^-$ anion radical coordinated to the divalent Ni(II) ion.[56,66] A single, strong IR band at 1506 cm^{-1} and a sharp δ(C−H) bending band at 825 cm^{-1} are consistent with the presence of the $TCNQ^-$ radical,[56,57] and not the $[TCNQ-TCNQ]^{2-}$ σ-dimer (δ(C−H) ≈ 802 cm^{-1}).[56] The presence of two broad IR bands at 3448 and 3375 cm^{-1}, along with a weak band at ∼1642 cm^{-1}, suggests that the electrochemically produced material contains coordinated water molecules[62] and that the product of reduction of solid TCNQ-modified electrodes is solid Ni[TCNQ]$_2$(H$_2$O)$_2$. This is fully confirmed by comparison of the IR data obtained by solid−solid conversions under different electrolysis conditions (see Table 4) with that found for an authentic sample of chemically synthesized Ni[TCNQ]$_2$(H$_2$O)$_2$[56]. In general, IR data show that conversion of solid TCNQ microparticles into the corresponding blue

(66) Khatkale, M. S.; Devlin, J. P. *J. Chem. Phys.* **1979**, *70*, 1851.

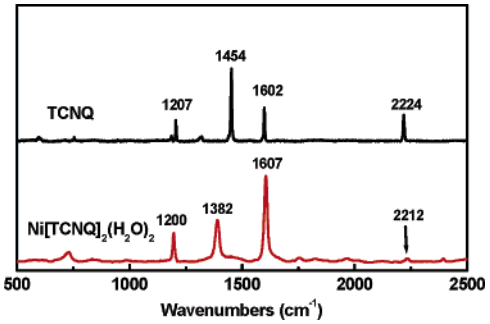

Figure 5. Raman spectra of solid TCNQ and $Ni[TCNQ]_2(H_2O)_2$ formed as a result of bulk electrolysis at $E_{appl} = -0.05$ V for 15 min when a TCNQ-modified ITO electrode (drop cast method) is in contact with 0.1 M $Ni(NO_3)_{2(aq)}$ electrolyte.

$Ni[TCNQ]_2(H_2O)_2$ solid is achieved electrochemically (Table 4) using the procedures described in this study.

II.B. Raman Spectroscopy. The Raman spectra of solid TCNQ crystals and the solid generated by electrolysis at $E_{appl} = -0.05$ V for 15 min of a TCNQ-modified ITO electrode (drop cast) are presented in Figure 5. Clearly, the four intense Raman vibrations obtained from TCNQ at 1207, 1454, 1602, and 2224 cm^{-1} are affected by reduction to $TCNQ^-$ and subsequent coordination to Ni(II). In particular, the band at 1454 cm^{-1}, attributed to the C═C ring stretching mode of TCNQ, is replaced by a new broad band at lower energy (1382 cm^{-1}). The red shift in this band of 72 cm^{-1}, found after reduction, is consistent with that expected for formation of the hydrated $Ni[TCNQ]_2(H_2O)_2$ complex and is also similar to that reported for formation of other MTCNQ complexes, (M = Cu, Ag, or alkali metals).[66−69] This shift confirms the presence of coordinated $TCNQ^-$ in the generated material and also the formation of the hydrated phase. The shift of 12 cm^{-1} for the 2224 cm^{-1} band to lower energy, along with a reduction of its intensity,[69] provides an additional Raman fingerprint for the formation of $Ni[TCNQ]_2(H_2O)_2$.

II.C. Energy-Dispersive X-ray. EDAX elemental analysis of solids formed at TCNQ-modified ITO electrodes by either reductive electrolysis or cyclic voltammetry confirmed the presence of Ni, as well as carbon and nitrogen, as expected for the formation of $Ni[TCNQ]_2(H_2O)_2$.

The combined electrochemical and spectroscopic (IR, Raman, and EDAX) data imply that when microcrystals of TCNQ are immobilized on the working electrode surface (GC, Pt, Au, ITO) and then reduced in the presence of Ni^{2+}-(aq) electrolyte ions, only the hydrated $Ni[TCNQ]_2(H_2O)_2$ phase is formed via a nucleation/growth process.

III. SEM Probing of the Morphological Changes Associated with the Redox-Induced TCNQ/$Ni[TCNQ]_2(H_2O)_2$ Transformation. Figure 6a shows an SEM image of a typical rhombus-shaped crystal (40 × 40 μm) of TCNQ initially immobilized on the surface of an ITO electrode via the drop casting method. SEM images obtained after $Ni[TCNQ]_2(H_2O)_2$ is formed, when this TCNQ-modified ITO

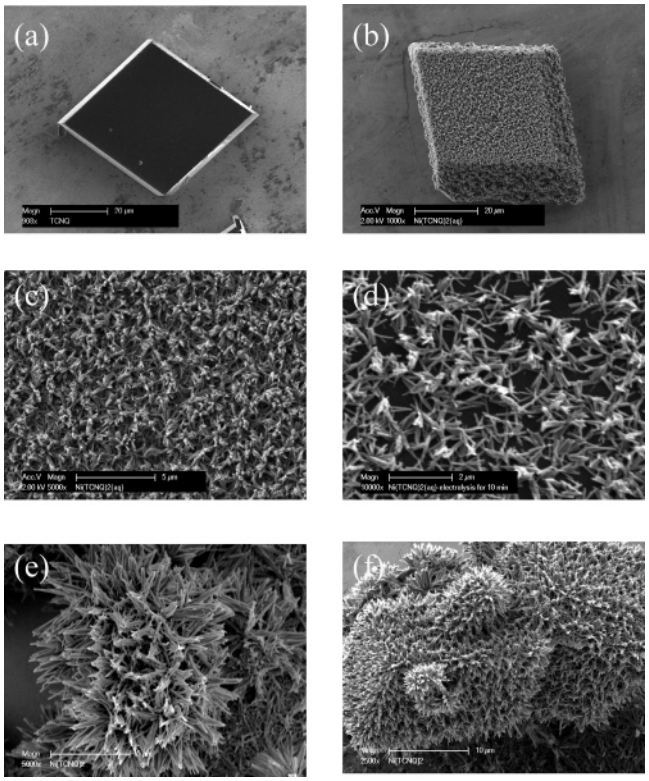

Figure 6. (a) SEM image of a single crystal of TCNQ present on a TCNQ-modified ITO electrode prepared via the drop casting method. (b) SEM image of $Ni[TCNQ]_2(H_2O)_2$ formed by reductive electrolysis for 10 min at −0.05 V of a crystal as shown in panel a when the TCNQ-modified ITO electrode is immersed in 0.1 M $Ni(NO_3)_{2(aq)}$ electrolyte. (c) Top view of the crystal shown in image b at a higher magnification. (d−f) $Ni[TCNQ]_2(H_2O)_2$ nanowires formed from reduction of other TCNQ crystals present on different regions of the electrode surface.

electrode is placed in contact with 0.1 M aqueous solution of $Ni(NO_3)_2$ electrolyte and then subjected to 10 min of reductive electrolysis at $E_{appl} = -0.05$ V vs Ag/AgCl, are provided in Figure 6b−f. During the reductive electrolysis, the surface of the parent large-sized TCNQ crystals become completely covered with nanosized $Ni[TCNQ]_2(H_2O)_2$ crystals (see for example, Figure 6b, low-magnification). High magnification (Figure 6c and d) SEM images reveal that these nanosized architectures consist of a network of densely packed, 2-D/3-D nanowires/nanorods having an average size of 500 nm to 1.0 μm in length and ∼50−100 nm in diameter. Interestingly, SEM images obtained from some regions of the ITO electrode surface (Figure 6e and f), probably where smaller parent TCNQ crystals are initially present, gave rise to $Ni[TCNQ]_2(H_2O)_2$ nanowires having a preferred orientation in which their tips prominently point upward to produce "sea urchin-like" structures (see Figure 6e). Formation of $Ni[TCNQ]_2(H_2O)_2$ in the form of a nanowire/nanorod network, via reduction of TCNQ-modified electrodes (drop cast), normally leaves the characteristic overall rhombus shape of the parent TCNQ structure intact provided that the parent TCNQ crystal is significantly large and the electrolysis time sufficiently short (10 min or less). The fact that the majority of nanowires (Figure 6b) are preferentially derived from the growth along the surface (edges, top and presumably base) of the large TCNQ crystals rather than through the middle allows the basic

(67) Kamitsos, E. I.; Risen, W. M., Jr. *J. Chem. Phys.* **1983**, *79*, 5808.
(68) Liu, S.-G.; Liu, Y.-Q.; Zhu, D.-B. *Thin Solid Films* **1996**, *280*, 271.
(69) Ye, C.; Cao, G.; Fang, F.; Xu, H.; Xing, X.; Sun, D.; Chen, G. *Micron* **2005**, *36*, 461.

architecture to remain intact. From an energetic point of view, the triple phase solid|electrode|electrolyte interface[59] probably produces the location for initial nucleation sites, which would then preferentially grow from the base of TCNQ crystal along the edges of the TCNQ crystal. This type of nanowire network nucleation/growth is promoted by the semiconducting nature of the $Ni[TCNQ]_2(H_2O)_2$ material,[49,51] which effectively increases the area of the electrode surface as crystal growth extends. Thus, substantial nucleation and growth also may occur on the top part of the TCNQ crystal as time proceeds. Growth into the interior of large TCNQ crystals may be restricted by the iR_u drop.

Reductive electrolysis experiments at ITO surfaces modified with solid TCNQ using the mechanical attachment method resulted in dramatically different morphologies for both parent TCNQ (Figure 7a) and generated $Ni[TCNQ]_2(H_2O)_2$ crystals (Figure 7b and c). As can be seen in Figure 7a, upon reductive electrolysis for 10 min, the densely packed "thin layer" of small TCNQ particles are converted into a compact layer of vertically aligned nanosized crystals (Figure 7b) or into bundles of needle-shaped $Ni[TCNQ]_2(H_2O)_2$ structures (Figure 7c) having an average length of about 2 μm and a diameter of about 100 nm in their middle section.

SEM images obtained when mechanically attached TCNQ-modified ITO surfaces were subjected to the conditions of cyclic voltammetry (10.5 cycles of the potential over the range from 0.35 to -0.05 V) and in the presence of 0.1 M $Ni^{2+}_{(aq)}$ electrolyte also reveal the existence of a drastically different kind of morphology for the generated $Ni[TCNQ]_2(H_2O)_2$ crystals to that found when exhaustive reductive electrolysis is employed to induce the transformation process. At lower magnification (Figure 8a), solid $Ni[TCNQ]_2(H_2O)_2$ material, formed under conditions of cyclic voltammetry, exhibits relatively uniform flower-shaped architectures. Although the majority of these structures are observed as flowerlike aggregates, some are detected as separated single flowerlike architectures. Analysis of the 3-D flowerlike $Ni[TCNQ]_2(H_2O)_2$ architectures, using high-resolution images such as those in Figure 8b and 8c, implies that each nanoarchitecture is composed of radially oriented, tapered-tip nanowires $\sim$2 μm in length and $\sim$50$-$100 nm in diameter, which are probably derived from nanosized TCNQ particles. The crystal shape (morphology) and size associated with $Ni[TCNQ]_2(H_2O)_2$ generated under cyclic voltammetric conditions may be attributed to the progressive changes induced by multiple occurrences of the chemically reversible TCNQ/$Ni[TCNQ]_2(H_2O)_2$ transformation. During the initial reductive (negative) potential direction scan, TCNQ particles (see Figure 7a) are converted into 3-D flowerlike $Ni[TCNQ]_2(H_2O)_2$ nanowire architectures by inclusion of $Ni^{2+}_{(aq)}$ ions from the bulk solution into the $TCNQ^-$ lattice. Reoxidation of the reductively formed $Ni[TCNQ]_2(H_2O)_2$ when the potential is scanned in the positive direction leads to the generation of TCNQ nanoparticles that are even smaller than those that were initially present (see Figure 8a). Repeated cycling of the potential ultimately leads to better defined and more uniform sizes of very small crystals of both TCNQ and $Ni[TCNQ]_2(H_2O)_2$.

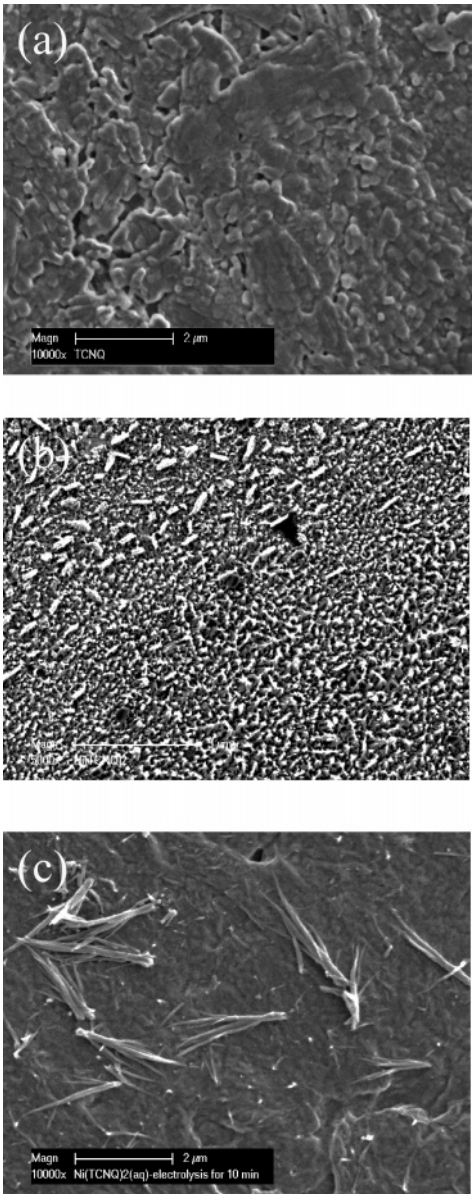

Figure 7. (a) SEM image of a TCNQ-modified ITO electrode (the mechanical attachment method). (b) SEM image of $Ni[TCNQ]_2(H_2O)_2$ formed by reductive electrolysis for 10 min at -0.05 V of solid TCNQ adhered to an ITO electrode surface (mechanical attachment method) after being placed in contact with 0.1 M $Ni(NO_3)_{2\ (aq)}$ electrolyte.

The morphology changes that accompany transformation of $Ni[TCNQ]_2(H_2O)_2$ back to TCNQ under reductive$-$oxidative bulk electrolysis conditions with TCNQ-modified ITO via mechanical attachment was also monitored via SEM. In this situation, SEM images (Figure 9) of TCNQ obtained after back oxidation of the blue $Ni[TCNQ]_2(H_2O)_2$ material, formed initially upon reductive electrolysis show the characteristic morphology expected for TCNQ crystals, namely, dispersed nanosized cubic/rhombus shaped yellow crystals. This represents a significant difference to the compact layer of TCNQ particles initially present (Figure 7a). Thus, TCNQ crystals need to fragment and hence undergo a net decrease in size to accommodate the different morphologies of TCNQ and $Ni[TCNQ]_2(H_2O)_2$ forms during the course of exhaustive

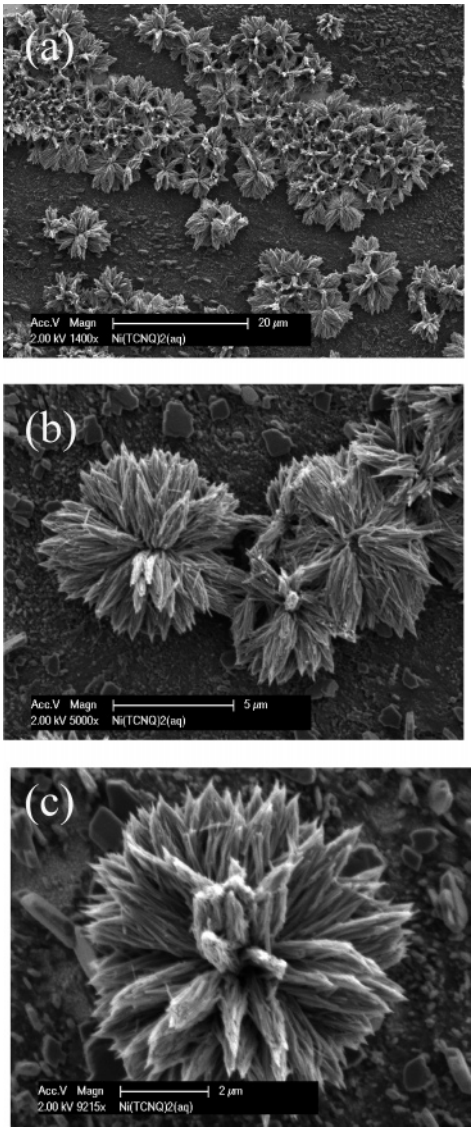

Figure 8. SEM images at progressively higher magnifications obtained after completion of 10.5 cycles of potential at a scan rate of 20 mV s^{-1} over the range from 0.35 to −0.075 V with a TCNQ-modified ITO electrode (mechanical attachment method) in contact with 0.1 M $Ni(NO_3)_{2\ (aq)}$ electrolyte.

bulk reduction−oxidation sequences. IR spectra of the solid produced by back-oxidation revealed the characteristic bands at 2228, 1543, and 860 cm^{-1} expected for TCNQ,[66] thereby confirming that regeneration of TCNQ does occur under these conditions.

Taken together, the SEM findings clearly establish that the morphology and crystal size of the electrochemically produced $Ni[TCNQ]_2(H_2O)_2$ material are strongly dependent on both the method of electrode modification with solid TCNQ (drop cast vs mechanical attachment) and on the voltammetric technique used to induce the TCNQ/Ni-$[TCNQ]_2(H_2O)_2$ solid−solid transformation. Furthermore, significant differences in morphologies and crystals sizes obtained for isostructural $Co[TCNQ]_2(H_2O)_2$[62] and Ni-$[TCNQ]_2(H_2O)_2$ complexes, under similar conditions, confirm that the nature of the cation controls the extent and direction of growth in redox-based interconversion of these nanostructured materials.

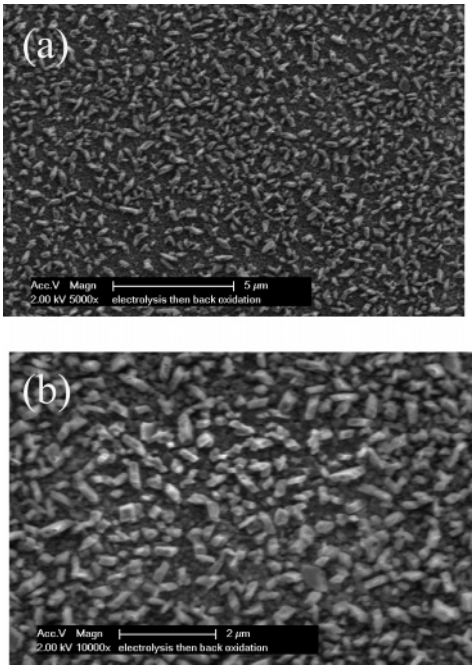

Figure 9. SEM images at (a) low and (b) high magnification showing the morphology of microcrystals of TCNQ formed after the sequence of reductive electrolysis of a TCNQ-modified ITO electrode (mechanical attachment method) at $E_{appl} = -0.05$ V for 10 min when it was placed in contact with the $Ni(NO_3)_{2(aq)}$ electrolyte to form $Ni[TCNQ]_2(H_2O)_2$, followed by oxidative back electrolysis to regenerate TCNQ at $E_{appl} = 0.4$ V for 10 min.

IV. Mechanistic Considerations of the TCNQ/Ni-$[TCNQ]_2(H_2O)_2$ Transformation Process. Voltammetric, spectroscopic, and microscopic data, when considered in combination, demonstrate that formation of blue solid Ni-$[TCNQ]_2(H_2O)_2$ nanowires occurs via a nucleation/growth mechanism when rhombus-shaped TCNQ crystals adhered to an electrode surface are reduced by one-electron to the corresponding $TCNQ^-$ radical anion in the presence of an aqueous solution of $Ni^{2+}_{(aq)}$ ions. The overall two-electron charge-transfer process is represented by eq 6. Because the

$$2[TCNQ]_{(s,GC,ITO)} + Ni^{2+}_{(aq)} + 2e^- \overset{H_2O}{\rightleftharpoons} \{Ni[TCNQ]_2(H_2O)_2\}_{(s,GC,ITO)} \quad (6)$$

$Ni^{2+}_{(aq)} + 2e^- \rightarrow Ni^0$ reduction in aqueous media ($E_p^{red} \geq 1.0$ V) is more negative than both of the $TCNQ^{0/-/2-}$ processes, the $Ni^{2+}_{(aq)}$ ions are most likely to be involved only in the charge neutralization step and not in the electron-transfer process. In the case of the TCNQ to CuTCNQ interconversion, $Cu^{2+}_{(aq)}$ ions present in bulk solution participate in both processes.[45] Moreover, the morphology of the electrogenerated $Ni[(TCNQ]_2(H_2O)_2$ complex is highly dependent on the method of electrode modification, that is, the initial TCNQ crystal size and morphology, and the necessity to accommodate the requirements of conversion of basically rhombus-shaped TCNQ microcrystals to needle-shaped $Ni[TCNQ]_2(H_2O)_2$ nanowires that needs to occur during the solid−solid redox based transformation.

Conclusions

Facile electrochemical approaches have been developed to induce the chemically reversible, redox-based, solid−solid

phase transformation of TCNQ microcrystals into nanowire/nanorod or flowerlike architectures of the semiconducting and magnetic $Ni[TCNQ]_2(H_2O)_2$. This TCNQ/$Ni[TCNQ]_2(H_2O)_2$ interconversion process uses the reduction of solid TCNQ into $TCNQ^-$ as a key step followed by the incorporation of $Ni^{2+}_{(aq)}$ ions from the bulk solution into the crystal lattice. The conversion process involves the overall transfer of two-electron charge transfer and is governed by initial nucleation at the triple-phase TCNQ|electrode|electrolyte interface followed by rapid growth kinetics. The voltammetric behavior is independent of electrode material and identity of Ni(II) counteranions but exhibits a marked dependence on the method of electrode modification, as well as on the scan rate and the concentration of the $Ni^{2+}_{(aq)}$ electrolyte. The identity of the electrochemically generated $Ni[TCNQ]_2(H_2O)_2$ material formed by reduction of solid TCNQ has been confirmed by IR, Raman, and EDAX techniques. SEM images obtained for the as-prepared $Ni[TCNQ]_2(H_2O)_2$ nanoarchitectures revealed that their morphology can be manipulated to yield either needle-shaped nanowires or flowerlike networks depending on the method of TCNQ−surface immobilization and the voltammetric technique employed. A potential outcome is access to superior electrochemical routes to control the synthesis and crystal growth of the aqueous $Ni[TCNQ]_2(H_2O)_2$ complex than provided by chemical methods.

Acknowledgment. Financial support from the Australian Research Council is gratefully acknowledged. The authors express their appreciation to Dr. Alexander Bilyk, Steven Pentinakis, and John Ward from the CSIRO Division of Manufacturing and Materials (CMMT) for technical assistance and the SEM instrumentation used in these studies. We also wish to thank Dr. Anthony P. O'Mullane (Monash University) for helpful discussions.

Supporting Information Available: Two figures showing the dependence of voltammetric parameters (E_m, E_p^{red}, and E_p^{ox}) on $Ni^{2+}_{(aq)}$ concentration (Figure S1) and the IR spectrum (Figure S2) of $Ni[TCNQ]_2(H_2O)_2$ formed under conditions of repetitive cyclic voltammetry at a TCNQ-modified ITO using the mechanical attachment method. This material is available free of charge via the Internet at http://pubs.acs.org.

IC062470L